Characterizing Liquid Phase Fabric of Unsaturated Specimens from X-Ray Computed Tomography Images

Kalehiwot N. Manahiloh and Balasingam Muhunthan

Abstract. Pore-water in the funicular and pendular saturation regimes of the SWCC (Sr < 90%) assumes a complex fabric consisting of saturated pockets of water under negative pressure and a network of liquid bridges formed from menisci at the contact points of particles. Measurement and characterization of this liquid fabric for unsaturated soil assemblies over a range of saturation, stress, and deformation plays a pivotal role in improving our fundamental understanding of unsaturated soil behavior. However, lack of microstructural visualization techniques has hindered the consideration of liquid fabric distribution and evolution in macroscale geotechnical formulations. In this study X-ray CT scanning was used to monitor the changes in the liquid fabric of unsaturated glass beads. Images showing the three distinct phases of unsaturated specimens were successfully obtained. A computer code that automatically analyzes multiple images to quantify the components of a second-order fabric tensor was developed and applied to CT images obtained along the drying and wetting paths of a SWCC determined by digital image processing. Principal values, principal directions and invariants are quantified and implications of the changes to better description of unsaturated soil behavior are discussed.

Keywords: unsaturated soils, X-ray CT, fabric tensor, granular geomaterials, SWCC.

Kalehiwot N. Manahiloh
Washington State University, Pullman, USA
e-mail: knega@wsu.edu

Balasingam Muhunthan
Washington State University, Pullman, USA
e-mail: muhuntha@wsu.edu

1 Introduction

Most flow, stress and deformation related problems are influenced by the engineering properties of unsaturated soils (Lu & Likos 2004). Even though, a considerable research has been conducted in the past (Matyas & Radhakrishna 1968, Likos & Lu 2004, Lu & Likos 2004) further studies are crucially important to fully incorporate unsaturated soil mechanics into engineering practice. In addition, investigations need to include microstructural considerations over ranges of saturation, stress and deformation so as to resolve fundamental issues in unsaturated soil behavior. In this study, funicular and pendular saturation regimes of unsaturated granular media (see Fig. 1) are investigated at a microstructural level and attempts are made to characterize their liquid fabric distribution.

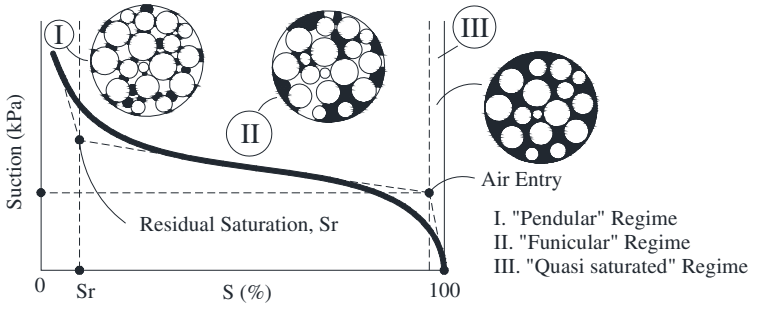

Fig. 1. Regimes of SWCC for partially saturated granular soil.

Nondestructive imaging techniques such as X-ray computed tomography (CT) have provided superior tools to quantitatively describe the 3-D microstructure of granular materials (Desrues et al. 1996, Wang et al. 2003, Gebrenegus et al. 2006). X-ray CT scanning combined with digital image processing can provide directional data and characterize microstructure of partially saturated specimens.

The objective of this study is to automate the handling of liquid phase fabric in X-ray CT images of unsaturated specimens and obtain their fabric tensor. Directional data gathered from X-ray CT scanning of 1mm glass beads at different suctions are digitally analyzed. The present interest is not to treat the complete theory covering unsaturated specimens, but rather to exemplify the use of image processing in quantifying directional data for phases of interest and combine the technique with statistical correlations to describe phase distribution.

2 Fabric Tensor of the Liquid Phase

Mathematically, *fabric* had been defined (Scott 1963, Mitchell 1976, Muhunthan 1991) in a number of ways and most researchers (e.g. Cowin & Satake 1978,

Nemat-Nasser & Mehrabadi 1983, Kanatani 1984, Kanatani 1985) studied fabric tensor for solid particles only. For two dimensional cases, Oda and Nakayama (1989) followed Kanatani's definition of fabric tensor and sought for measures by defining a vector along the longest chord of solid particles.

According to Muhunthan (1991), defining tensor parameters on the void phase have a potential of delivering a unified measure for all particulate media. Moreover, the advent of X-ray CT and its application to scanning of geomaterials has enabled to distinctly image the solid, liquid, and gas phases at a microstructural level. Therefore, in this study, fabric is accepted as a term referring to parameters like size, shape and arrangement of the solid particles, the organic inclusions and the associated voids. Also, statistical correlations applicable to solid particles are assumed to appropriately describe directional distributions on the liquid phase. Following the preceding discussion, this study will quantify higher measures of fabric on the liquid phase of a partially saturated specimen.

3 Mathematical Background for Fabric Tensor

Kanatani (1984) studied and gave mathematical expressions for quantities that characterize directional distribution of particles. The subsequent discussion revises the mathematical formulation of these quantities.

Assume directional data n that is observed for a material idealized as an assembly of solid spheres. Assume also, $f(n)$ is the *probability* distribution density satisfying $\int f(n)dn = 1$. Where, dn is the differential solid angle related to the spherical coordinates θ and ϕ as:

$$\int dn = \int_0^{\pi} \int_0^{2\pi} \sin\theta d\phi d\theta \quad \text{(For 3-D)} \quad (1) \qquad \int dn = \int_0^{2\pi} d\theta \quad \text{(For 2-D)} \quad (2)$$

To estimate the true distribution density, the singular distribution function, $f(n)$ is approximated by a smooth function $F(n)$. In this procedure a *parametric form* is first assumed and then a *measure of approximation* is introduced. Parameters are then chosen in such a way that the introduced measure of approximation is maximized. A polynomial parametric form of $F(n)$ (Kanatani 1984) can take the form given by equation (3) where the C terms represent coefficients.

$$F(n) = C + C_i n_i + C_{ij} n_i n_j + C_{ijk} n_i n_j n_k + \ldots \quad (3)$$

A measure of approximation, invariant to coordinate transformation, is given in equation (4) (Kanatani 1984) and is termed the *least square error approximation*. This approximation takes the polynomial parametric form to the spherical harmonics and the Fourier series expansions in the 3-D & 2-D cases respectively.

$$\int [F(n) - f(n)]^2 dn \rightarrow Minimum \quad (4)$$

Assuming a pair of unit vectors with opposite directions to be generated so that *f(n)*is a symmetric function (i.e. only even powers of *n* to be included), equations (3) and (4) can be combined such that the square error *E* is minimized, to obtain the following form.

$$E = \int [(C + C_{ij} n_i n_j + C_{ijkl} n_i n_j n_k n_k + ...) - f(n)]^2 dn \rightarrow Minimum \quad (5)$$

Kanatani (1984) approximated distribution functions for solid particles and gave expressions for fabric tensors of the *first*, *second* and *third* kind as expansions of relevant subspace. In three dimensional subspaces, for $n = 2$, the *second* (F_{ij}) and *third* (D_{ij}) kind reduce to equations (6) and (7) respectively. The corresponding tensor definitions in two dimensional subspaces are given by equations (8) and (9).

$$F_{ij} = \frac{15}{2}\left[N_{ij} - \frac{1}{5}\delta_{ij} \right] \quad (6) \qquad D_{ij} = \frac{15}{2}\left[N_{ij} - \frac{1}{3}\delta_{ij} \right] \quad (7)$$

$$F_{ij} = 4\left[N_{ij} - \frac{1}{4}\delta_{ij} \right] \quad (8) \qquad D_{ij} = 4\left[N_{ij} - \frac{1}{2}\delta_{ij} \right] \quad (9)$$

4 Experimental Setup

Spherical glass beads of 1mm were packed into a 10 mm diameter cylindrical plexiglass Tempe-cells that can maintain constant suction applied from a hanging water column. Samples were scanned with X-ray CT and digital image processing was applied on the resulting images. The liquid phase was systematically captured by doping the saturating fluid with 6% CsCl solution. The components of higher order fabric tensors and associated invariants are computed from image analysis. To illustrate the techniques applied, a two dimensional image shown in Fig. 2 is considered. In the figure, $n^{(k)}$ represents a unit vector aligned with the longest chord of the k^{th}-particle making an angle θ with respect to the horizontal axis.

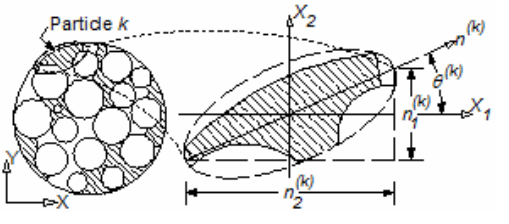

Fig. 2. Particle Orientation: (a) 2-D slice & global axes; (b) k^{th} particle, local axes, longest chord & fitting ellipsoid.

Decomposing the unit vector into its orthogonal components, one can obtain expressions for n_1 and n_2 as follows:

$$n_1 = \sin\theta^{(k)} \text{ and } \quad n_2 = \cos\theta^{(k)} \tag{10}$$

In each X-ray CT slice, the total number of data points (i.e. each liquid completely or partially surrounded by solid particles) for which directional data is sought is represented by M. Following Oda & Nakayama (1989) the components of the fabric tensor can be calculated as:

$$N_{11} = \frac{1}{M}\sum_{k=1}^{M}\sin^2\theta^{(k)} \tag{11}$$

$$N_{12} = \frac{1}{M}\sum_{k=1}^{M}\cos\theta^{(k)}\sin\theta^{(k)} \tag{12}$$

$$N_{22} = \frac{1}{M}\sum_{k=1}^{M}\cos^2\theta^{(k)} \tag{13}$$

Image Pro Plus platform is used to run a macro that handles the direction assignment, angle measurement and computations for components of the fabric tensor. A typical image from X-ray CT scanning is shown in Fig. 3a. AutoCAD simulation of the same image where the three independent phases (i.e. solid, liquid and gas) are distinctively represented is shown in Fig. 3b. In Fig. 3c the liquid phase is extracted and shown shaded. Fig. 3d shows the longest chords of each discretized liquid phase constituent. The samples considered for the analysis are summarized in Table 1 where each column has a heading that explains what is represented.

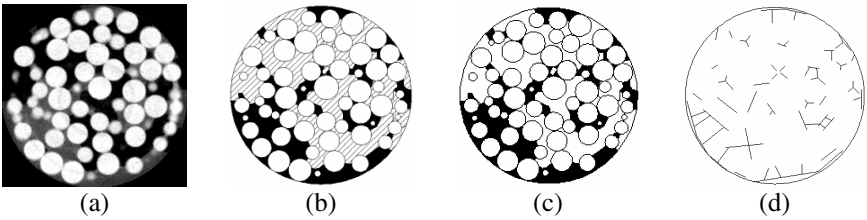

Fig. 3. Image from X-ray CT: (a) 1mm Glass Bead at suction of 0.6kPa (Drying); (b) All Phases: stripe = gas, black = liquid and white = solid; (c) Liquid Phase (black); (d) Longest chords of discretized liquid phases.

5 Results and Discussion

The distributions of N_{11}, N_{12} and N_{22} for sample 1 are shown in Figs. 4 through 6. These distributions were obtained by coding equations (11) to (13) into Image-Pro Plus platform and running on images. Average values for the distribution descriptors and their invariants are summarized in Table 2. From the results, the fundamental property of fabric tensors can be proven such that the first invariant, I_1, is always Unity. The invariants are plotted together (Fig. 7) to show their variation as a function of the sample preparation pressure.

Table 1. Sample details.

(1)	(2)	(3)		(4)	(5)	(6)	(7)
Sample	Suction (kPa)	Diameter		Height (mm)	Calibration mm/pixel	Cropping co-ordinates	Threshold for Liquid
		pixel	mm				
1	0.0	236	10	14.32	0.042	(0,0;236,236)	31-127
2	0.4	236	10	13.97	0.042	(0,0;236,236)	31-127
3	0.6	234	10	14.58	0.043	(0,0;234,234)	31-127
4	0.8	271	10	11.95	0.037	(0,0;271,271)	31-127
5	2.5	238	10	13.98	0.043	(0,0;238,238)	31-127

Table 2. Average values for N_{ij} and associated invariants.

Sample	Suction (kPa)	N_{11}	N_{12}	N_{22}	I_1	I_2
1	0	0.504	0	0.496	1.000	0.250
2	0.4	0.503	0	0.497	1.000	0.250
3	0.6	0.506	0	0.494	1.000	0.250
4	0.8	0.512	0	0.488	1.000	0.250
5	2.5	0.502	0	0.498	1.000	0.250

Following the previous assertion, N_{ij} is written in full as a symmetric second order tensor and the obtained values for sample 1 are indicated below.

$$\begin{bmatrix} N_{11} & N_{12} \\ N_{21} & N_{22} \end{bmatrix} = \begin{bmatrix} 0.504 & 0 \\ 0 & 0.496 \end{bmatrix} \tag{15}$$

Since N_{ij} is a symmetric second order tensor, the components can be converted to two principal values N_1 and N_2 in the corresponding principal directions. Their mathematical formulations and corresponding principal directions are given by equations (15) and (16).

$$\begin{bmatrix} N_1 \\ N_2 \end{bmatrix} = \frac{1}{2}[N_{11} + N_{22}] \pm \left[\frac{1}{4}(N_{11} - N_{22}) + N_{12}{}^2 \right]^{0.5} = \frac{1}{2}(1 \pm \Delta) \tag{15}$$

$$\begin{bmatrix} \theta_1 \\ \theta_2 \end{bmatrix} = \frac{1}{2} \arctan \frac{2N_{12}}{N_{22} - N_{11}} \tag{16}$$

Curray (1956) introduced an index measure that shows the intensity of a preferred orientation of particles. This measure, referred to as *the vector magnitude,* is given as equation (17).

$$\Delta = \frac{1}{M} \left[\sum_{k=1}^{M} \left(\cos 2\theta^{(k)} \right)^2 + \sum_{k=1}^{M} \left(\sin 2\theta^{(k)} \right)^2 \right]^{0.5} \tag{17}$$

The results for the principal values, principal directions and the vector magnitude values are summarized in Table 3.

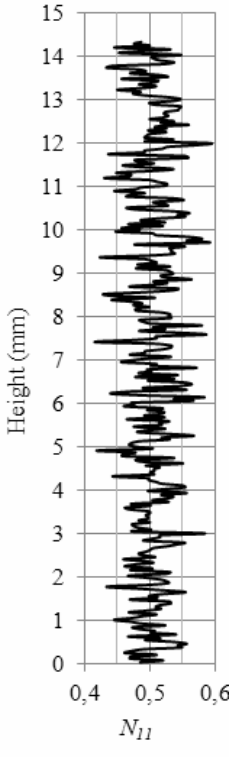

Fig. 4. N_{11} distribution over height.

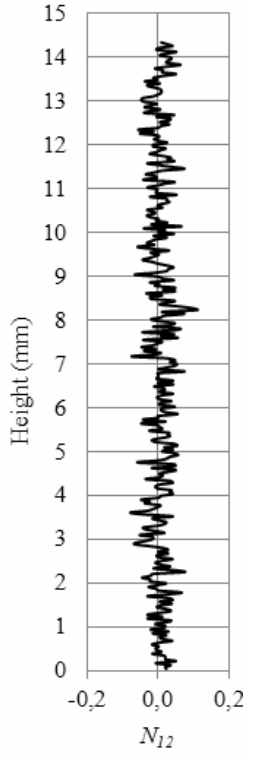

Fig. 5. N_{12} distribution over height.

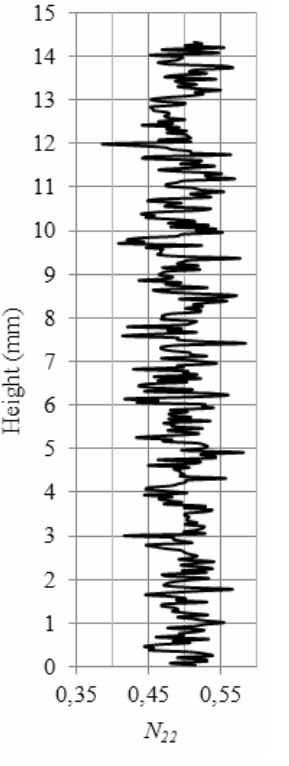

Fig. 6. N_{22} distribution over height.

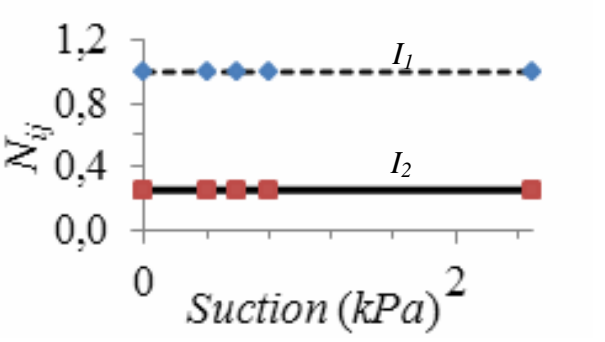

Fig. 7. Average N_{ij} values for all samples.

Table 3. Principal values, principal directions and vector magnitudes.

Sample	N_{11}	N_{12}	N_{22}	N_1	N_2	Δ	θ_1	θ_2
1	0.504	0	0.496	0.546	0.454	0.091	0	90
2	0.503	0	0.497	0.537	0.463	0.074	0	90
3	0.506	0	0.494	0.556	0.444	0.111	0	90
4	0.512	0	0.488	0.579	0.421	0.157	0	90
5	0.502	0	0.498	0.531	0.469	0.061	0	90

Table 4. Kanatani's fabric tensor of the *second* kind.

Sample	F_{11}	F_{12}	F_{22}	F_1	F_2	Δ
1	1.017	0	0.983	1.184	0.816	0.092
2	1.011	0	0.989	1.148	0.852	0.074
3	1.025	0	0.975	1.222	0.778	0.111
4	1.049	0	0.951	1.314	0.686	0.157
5	1.007	0	0.993	1.124	0.876	0.062

Table 5. Kanatani's fabric tensor of the *third* kind.

Sample	D_{11}	D_{12}	D_{22}	D_1	D_2	Δ
1	0.017	0	-0.017	0.184	-0.184	0.092
2	0.011	0	-0.011	0.148	-0.148	0.074
3	0.025	0	-0.025	0.222	-0.222	0.111
4	0.049	0	-0.049	0.314	-0.314	0.157
5	0.007	0	-0.007	0.124	-0.124	0.062

The relationship between F_{ij} and D_{ij} can be obtained from equations (8) and (9). The principal components of F_{ij} and D_{ij} can also be derived from these same equations and employing the representation indicated in equation (14), they can be written as equations (18) and (19). Tables 4 and 5 give their numerical values.

$$\begin{bmatrix} D_1 \\ D_2 \end{bmatrix} = \pm 2\Delta \quad (18) \qquad \begin{bmatrix} F_1 \\ F_2 \end{bmatrix} = 1 \pm 2\Delta = 1 + \begin{bmatrix} D_1 \\ D_2 \end{bmatrix} \quad (19)$$

6 Conclusions

This study presented an investigation on microstructural evolution of the anisotropic liquid fabric in unsaturated soils. Since void fabric and the liquid bridge vectors change dramatically with wetting and deformation, their characterization is important towards the development of effective stress formulations for unsaturated soils.

Second order fabric descriptors of the anisotropic liquid fabric are quantified from X-ray CT scanned images of unsaturated specimens. The results confirm that the liquid fabric is anisotropic and that the components satisfy the basic tensorial properties such as symmetry and equality of diagonal summation to unity. The results include principal values, principal directions, and vector magnitudes for the liquid fabric. These parameters can be used by researchers in developing advanced theories for modeling the behavior of unsaturated soils.

Acknowledgements. The study presented in this paper was sponsored by the National Science Foundation under the grant CMMI-0856793 to Washington State University.

References

Cowin, S.C., Satake, T.: Continuum mechanical and statistical approaches in the mechanics of granular materials, Tokyo, Japan, Gakujutsu Bunken Fukyu-Kai (1978)

Curray, J.R.: Analysis of two-dimensional orientation data. J. Geology. 64, 117–131 (1956)

Desrues, J., Chambon, R., Mokni, M., Mazerolle, F.: Void ratio evolution inside shear bands in triaxial sand specimen studied by computed tomography. Geotechnique 46(3), 529–546 (1996)

Gebrenegus, T., Tuller, M., Muhunthan, B.: The Application of X-ray computed tomography for characterization of surface crack networks in sand-bentonite mixtures. In: Proc. Advances in X-ray Tomography for Geomaterials, pp. 207–212. ISTE Publishing Company (2006)

Kanatani, K.I.: Distribution of Directional Data and Fabric Tensors. International Journal of Engineering Science 22, 149–164 (1984)

Kanatani, K.I.: Procedures for stereological estimation of structural anisotropy. International Journal of Engineering Science 23(5), 587–598 (1985)

Likos, W.J., Lu, N.: Hysteresis of capillary stress in unsaturated granular soil. Journal of Engineering Mechanics 130(6), 646–655 (2004)

Lu, N., Likos, W.J.: Unsaturated soil Mechanics. Wiley, New Jersey (2004)

Matyas, E.L., Radhakrishna, H.S.: Volume change characteristics of partially saturated soils. Geotechnique 18(4), 432–448 (1968)

Mitchell, J.K.: Fundamentals of soils behavior. John Wiley and sons, Inc., New York (1976)

Muhunthan, B.: Micromechanics of Steady State, Collapse and Stress-Strain Modeling of Soils. Ph.D. Thesis, 221 p. Perdue University, West Lafayette (1991)

Nemat-Nasser, S., Mehrabadi, M.M.: Stress and Fabric in Granular Masses. In: Jenkins, J.T., Satake, M. (eds.) Mechanics of Granular Materials: New Models and Constitutive Relations, pp. 1–8. Elsevier, Amsterdam (1983)

Oda, M., Nakayama, H.: Yield Function for soil with Anisotropic Fabric. Journal of Engineering Mechanics 115(1), 89–104 (1989)

Scott, R.F.: Principles of soil mechanics, pp. 267–275. Addison-Wesley Publishing Co. Inc., Massachusetts (1963)

Wang, L.B., Frost, J.D., Voyiadjis, G.Z., Harman, T.P.: Quantification of damage parameters using X-ray tomography images. Mechanics of Materials 35, 777–790 (2003)